JOURNAL OF GEOPHYSICAL RESEARCH, VOL. 114, D11111, doi:10.1029/2008JD011543, 2009

Polar mesospheric summer echoes at 78°N, 16°E, 2008: First results of the refurbished sounding system (SOUSY) Svalbard radar

C. M. Hall,[1] J. Röttger,[2] K. Kuyeng,[3] M. Tsutsumi,[4] M. Dyrland,[5] and J. L. Chau[3]

Received 20 November 2008; revised 26 February 2009; accepted 13 April 2009; published 6 June 2009.

[1] The second-generation sounding system (SOUSY) 53.5-MHz mesosphere-stratosphere-troposphere (MST) radar at 78°N, 16°E on Svalbard has recently completed its inaugural summer, 2008, of polar mesospheric summer echoes (PMSE) observations. Here PMSE observations have been assembled in order to identify dates of the earliest and latest occurrences and how the frequency of PMSE occurrence correlates with dynamics and temperature, which are available from the collocated Nippon/Norway Svalbard Meteor 31-MHz Radar (NSMR). We find strong correlations between preferred PMSE altitude and low temperature, and between equatorward flow and occurrence rate. Temperature drops cause increases in PMSE occurrence: for the height interval 82–92 km, a drop of around 7 K increases the occurrence, typically by 1–2% d^{-1} and similarly for a 1 m s^{-1} increase in equatorward wind. A temperature drop of 5 K at 90 km altitude results in a lowering of the underlying preferred PMSE altitude by 1 km. This study therefore qualifies, at least for 78°N, 16°E and 2008, the dependence of PMSE occurrence rates and preferred heights on 90 km temperature and dynamics.

Citation: Hall, C. M., J. Röttger, K. Kuyeng, M. Tsutsumi, M. Dyrland, and J. L. Chau (2009), Polar mesospheric summer echoes at 78°N, 16°E, 2008: First results of the refurbished sounding system (SOUSY) Svalbard radar, *J. Geophys. Res.*, *114*, D11111, doi:10.1029/2008JD011543.

1. Introduction and the SSR2 Radar

[2] A striking feature of radar observations of the middle atmosphere, particularly at VHF, is the occurrence of strong echoes often appearing as discrete layers at preferred heights. Such echoes can appear at any time of the year and any latitude and a number of acronyms have been devised to refer to them. Here we report observations of polar summer mesospheric echoes (PMSE), which, as the name indicates are phenomena pertaining to the high-latitude mesosphere. Furthermore, also as indicated by the name, these are radar phenomena and can be thought of a priori in the same way as a rainbow; a rainbow does not exist without the eye to perceive it, and similarly neither does a PMSE without a radar. Even so, these echoes exhibit various characteristics which can yield information on processes in the atmosphere, including, potentially, climate change. While *Ecklund and Balsley* [1981] are often honored with the first reports of such echoes at high latitude, *Czechowsky et al.* [1979] had also reported more general observations a little earlier. A feature of the high-latitude mesopause region in summer, whence PMSE are observed, is that it is the coldest part of the atmosphere and these low temperatures are, in part, responsible for the strong radar echoes. Rather than launch into a review of current PMSE theory, the reader is referred to *Rapp and Lübken* [2004]. In summary, real structures in the mesopause region are made visible to radar by a population of charged particles with considerably greater inertia than normal ionospheric constituents (variously: hydrated ions, macroions, charged dust or ice, depending on the theory in favor). As an example, in one theory [*Kelley et al.*, 1987], such heavy charged particles could be responsible for high Schmidt numbers, i.e., reduced electron diffusion, leading to PMSE at VHF; high Schmidt numbers signify that turbulent structures in the electron gas can exist in the tracer responsible for gradients in refractive index, that would otherwise be damped out by viscosity. To resolve such theories, several in situ investigations have attempted to determine the aeronomy in the regions where PMSE occurs, a recent study being that of *Brattli et al.* [2009], such that we are now reaching a better understanding of the echo mechanism. Previous PMSE studies include those of *Ecklund and Balsley* [1981] (mentioned above), *Latteck et al.* [2008] (and references therein), and, not least from Svalbard, *Hall and Röttger* [2001], *Lübken et al.* [2004] and *Röttger et al.* [2007].

[3] The second-generation SOUSY 53.5-MHz MST radar at 78°N, 16°E on Svalbard (SSR2) represents a new addition to the arsenal of instruments capable of detecting PMSE, superseding the original SOUSY system. Its value lies in its high-latitude location and its ability to run unattended, thus monitoring PMSE occurrence. Here we exploit this continual monitoring to examine how occurrences at various heights

[1] Tromsø Geophysical Observatory, University of Tromsø, Tromsø, Norway.
[2] Max Planck Institute for Solar System Research, Katlenburg-Lindau, Germany.
[3] Radio Observatorio de Jicamarca, Instituto Geofisico del Peru, Lima, Peru.
[4] National Institute of Polar Research, Tokyo, Japan.
[5] University Centre in Svalbard, Longyearbyen, Norway.

0148-0227/09/2008JD011543$09.00

Table 1. SSR2 System Parameters

Parameter	Value
Frequency (MHz)	53.5
Antenna: number of four-element Yagis	356
Antenna gain (dBi)	30
Half-power beam width (degrees)	5
Peak power (kW)	1
Duty cycle (%)	8.7
Range resolution (m)	150
Pulse complementary coding	64 bit

and times relate to independently estimated temperatures and winds, and all at a higher latitude than the majority of previous observations.

[4] The SOUSY system [*Röttger*, 2001] is located in Adventdalen near Longyearbyen colocated with the 31-MHz Nippon/Norway Svalbard Meteor Radar (NSMR) [*Hall et al.*, 2002] and in close proximity to the EISCAT Svalbard Radar (ESR) [*Wannberg et al.*, 1997] and SPEAR (an ionospheric heater and HF radar) [*Robinson et al.*, 2006] systems. Also important are nearby optical instruments which, as we shall see, have been invaluable for providing temperature information in combination with NSMR (namely, LIDAR measurements by *Höffner and Lübken* [2007] and hydroxyl measurements described here). The original SOUSY radar has been refurbished in such a way as to be able to operate unattended with a high degree of reliability, though at very low transmitter power of 1 kW, and commenced regular operation in late summer 2007. Here, we shall present results from the first complete summer, 2008, of PMSE observations with the new system: SSR2, operating all day, every day, has been able to observe the onset of the Svalbard PMSE season and also its demise, together with simultaneous troposphere soundings (to be discussed elsewhere). The NSMR, also operating in an unattended mode, provides corresponding information on temperatures and horizontal winds, primarily at 90 km altitude.

[5] Since SSR2 is a relatively new installation, is innovative and not yet completely documented, we shall begin with a review of the system. The original SOUSY radar on Svalbard [*Röttger*, 2001] was designed to operate with a typical peak power of 70 kW and transmitting in steerable beams through a phased array of 356 four-element Yagis. Owing to the relatively high power consumption, operation was normally on a campaign basis, but by using the 4-kW driver and not the final amplifier, it was possible to achieve unattended operation. Because of the system design, however, operator intervention was still often required and, owing to an aging system, it was decided to improve reliability at the cost of flexibility and power, work being completed in late summer 2007. The refurbished system, SSR2, still uses the original antenna array and frequency (53.5 MHz), although without beam steering: only a vertical beam is used, this having a half power full width of 5°. The antenna beam is assumed to be widened from the original 4° to 5° owing to a fraction of the Yagi antennas being partially damaged owing to snow drift. The transmitter has been replaced by a 1-kW peak solid state unit supplied by Vikas (India) operating at 53.5 MHz and a second unit is currently available to either double the power or to provide redundancy. The radar controller, receiver and data acquisition system, consisting of a digital receiver based on off-the-shelf components, and modern PC are all new. All components can be controlled over the Internet but normally the system runs without any intervention whatsoever. The normal mode of operation is one of 20-min interlaced troposphere/lower stratosphere and mesosphere soundings and this resulting data set is unprecedented for this high-latitude geographic location. Furthermore, the price tag has been exceptionally low: excepting the antenna array which is part of the original SOUSY installation on Svalbard, the radar controller and major parts of the receiver system were developed and built at Jicamarca Radio Observatory (JRO). The redesign of the SOUSY Svalbard radar is about equivalent to that of the other SOUSY VHF radar, which is now located at the JRO, and described by *Woodman et al.* [2007]. Table 1 summarizes SSR2's operating characteristics for this particular experiment.

[6] We shall not discuss the troposphere mode in this study but rather focus on the PMSE observations made using the mesosphere mode. This mesosphere experiment samples from 81 km to 92 km altitude at 150 m resolution using a 64-bit complementary code at 8.7% duty cycle. While the system does store raw data (typically 0.5 GB/d mesosphere data), it is more convenient to postintegrate/analyze online yielding, for our purposes here, 5-min power profiles. These 5-min power profiles are therefore our starting point for what follows: we shall (1) examine occurrence rates and heights, (2) make quantitative comparisons between the PMSE statistics (for 2008) and atmospheric parameters determined by meteor wind radar, and finally (3) give an appraisal of our interpretation in terms of underlying physics.

2. Results

[7] Many examples of PMSE, particularly as time-height contour plots have been published earlier, thus, we show only one typical example of a PMSE height-time-intensity plot (Figure 1). PMSE exhibits diurnal variation in both occurrence and altitude, the former being mainly driven by tides and the latter by a wider range of dynamics scales and the temperature structure. The general pattern is then modulated by the degree of ionization, since at VHF, refractive index depends on electron density, but in particular on small charged ice particles, which form in the cold mesopause region [e.g., *Cho and Röttger*, 1997; *Brattli et al.*, 2009] described earlier. For each day, we have determined the percentage of time and observed height interval exhibiting PMSE, defined for our purposes as mesospheric signal 5 dB over the background noise level. Taking Figure 1 as an example, the daily occurrence is obtained by counting all pixels indicating a signal of $\geq$5 dB and dividing by the total number of pixels in the plot (here a ''pixel'' implies a rectangle having width = 5 min and height = 150 m). The 90-km rate is obtained similarly but by counting pixels corresponding to the 90-km radar gate only. As we shall see, the frequency of occurrence builds up rapidly following the initial appearance in late May and eventually tails off during August. In addition, we have determined the preferred altitude for each day by identifying the altitude of the maximum of the daily cumulative occurrence profile. Meteors are often seen by the radar and, despite filtering, these and other events may be mistakenly interpreted as PMSE during the automatic processing of the data. The

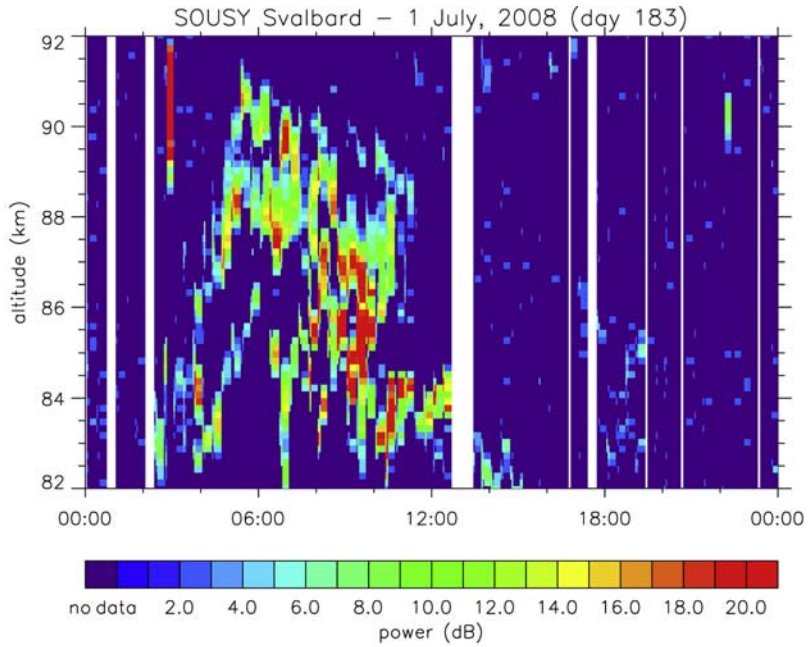

Figure 1. Typical PMSE, here from 1 July 2008, showing 24 h of mesospheric soundings as described in the text. White stripes indicate interruptions in operation, for example due to air traffic. Strong isolated features at 90 km such as those at 0300 and 2200 UT are meteor echoes. Any discernible 20-min fluctuations are manifestations of occasional troposphere-mesosphere mode switching problems.

statistics have therefore been screened and corrected manually where necessary.

[8] In parallel to the SSR2 backscattered power observations, NSMR has been used to estimate neutral temperatures from the fading times of meteor train echoes at 90 km altitude [*Hall et al.*, 2006]. These authors developed a method specific to NSMR and descriptions of more general methods are given by *Hocking* [1999] and *Holdsworth et al.* [2006]. Rather than attempt to obtain temperatures from the meteor radar data alone in combination with a model atmosphere, our philosophy has been to determine the ambipolar diffusion of the meteor trail ions and combine this with a model pressure (as described by *Holdsworth et al.* [2006]). We subsequently calibrate these estimates using independent measurements obtained from optical instruments. The majority of optical measurements, particularly more recent than those of *Hall et al.* [2006], are from winter and therefore the temperatures given in this study must be regarded as very approximate (contemporary research is correcting this shortcoming). The resulting daily absolute mean values are therefore only as good as the (relatively) very intermittent time series from the optical measurements. Thus, the temperature derivation used here is that of *Hall et al.* [2006] but incorporating more recent OH rotational temperature observations from instrumentation less than 5 km from the radar site [*Dyrland and Sigernes*, 2007] (also Dyrland et al. recent unpublished work). Although additional measurements are from winter days, they still the improve the overall meteor radar calibration.

[9] Even though the absolute values are uncertain, the relative temperature variation during summer 2008 is of considerable interest here. For each day SOUSY radar data were available (with or without PMSE), the corresponding mean temperature was obtained from NSMR. That the temperatures are derived for 90 km altitude (this being the height of the maximum meteor trail echo occurrence) is our reason for determining the percentages of each day for which PMSE are present at 90 km. Again, following the automatic processing of the radar data, the results have been screened and corrected manually where necessary. The results are shown in Figure 2. The overall PMSE occurrence (all observed heights and 24 h) is seen in Figure 2a, that for 90 km only in Figure 2b, the preferred PMSE altitude in Figure 2c, and lastly the temperature estimate in Figure 2d. Rather than indicate the absolute dates, the axes indicate day number relative to solstice (20 June for 2008). The preferred heights show considerable fluctuation toward the end of the period and this is due to the disappearance of PMSE and therefore the height becoming less easy to identify. All PMSE time series have been smoothed with a 10-day Lee filter [*Lee*, 1986], shown in addition. Temperatures have been smoothed by a 30-day Lee filter to reduce large fluctuations occurring before and after the PMSE window. At temperatures below the frost point ice particles can form. The dashed line at 134 K is the frost point temperature given by *Lübken et al.* [2004] using water vapor concentrations from *von Zahn and Berger* [2003] appropriate for solstice. The significance of the dotted line at 120 K in Figure 2d will be discussed later. It should be noted, however, that these temperatures (134 K and 120 K) both depend on water vapor saturation, a quantity that changes with both season and altitude, including through the PMSE regime. Water vapor has not been comprehensively measured in the mesosphere, let alone at high latitude, and so the indications in Figure 2 are very approximate and should largely be regarded as illustrative only.

[10] The first PMSE of the season observed with SSR2 was on 22 May. We have to note that the detectability depends on the power-aperture product of the observing radar and, thus, the initial day of PMSE observations may deviate by a few

days. The occurrence rose sharply during the subsequent 4 weeks maximizing just after solstice. Thereafter, occurrence tailed off more gradually and the last PMSE were observed on 25 August. The occurrence rate at 90 km is more temporally symmetric centered on the end of June, but there again, the majority of echoes occur below this height (recall we have selected 90 km especially only because it coincides with the meteor radar observations we shall use). The preferred height was also lowest nearer the midpoint of the observation season. It is interesting to note that the daily maximum never occurred above 89 km, whereas the lowest echoes observed were at the lowest heights for the experiment, namely, 82 km.

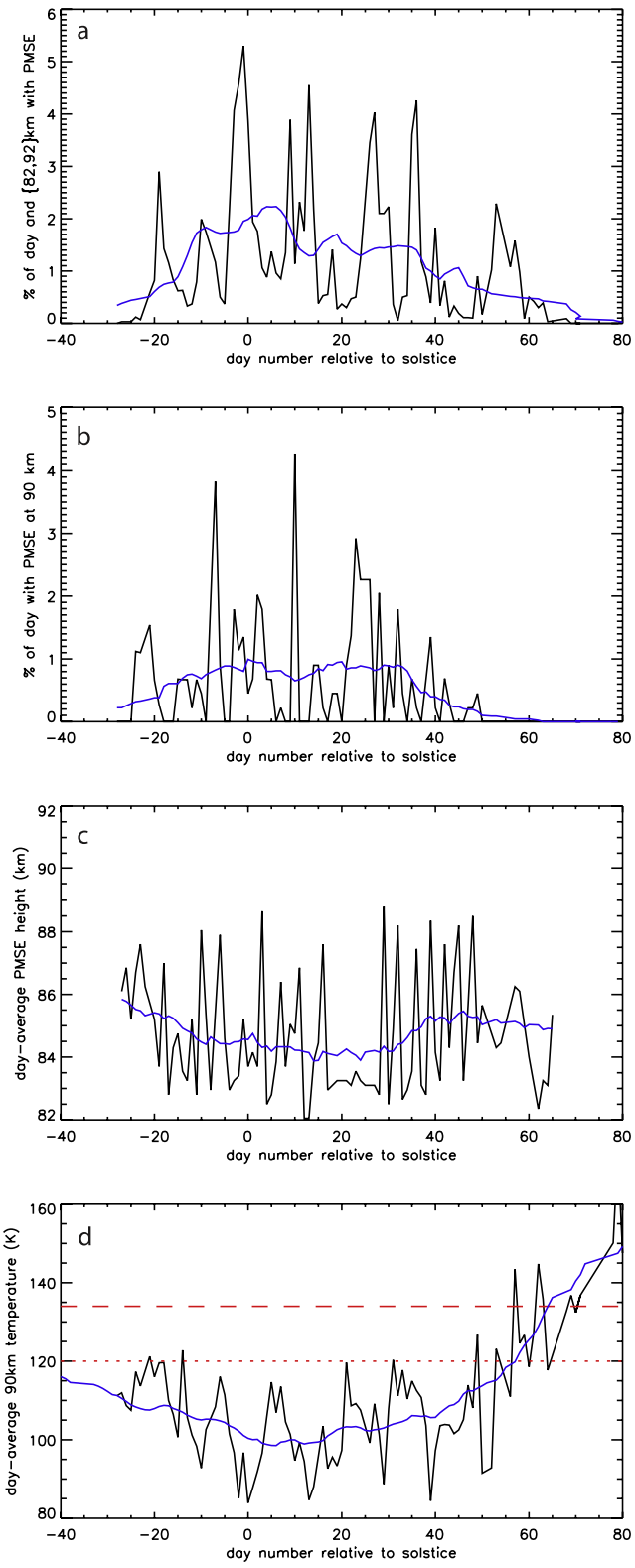

Figure 2. PMSE characteristics for 2008, determined by the SSR2 radar. (a) As a percentage of the day and of the 82–92 height interval covered by the SSR2 observation. (b) Daily PMSE occurrence but for 90 km altitude only. (c) Daily preferred PMSE height. (d) Partly calibrated (and therefore approximate) neutral temperatures obtained at 90 km altitude as determined by meteor wind radar (NSMR); the dashed line indicates a suggested frost point, and the dotted line is a suggested Kelvin barrier (see text). In all cases a smoothed (Lee filter) line is shown better illustrating overall variation through the summer.

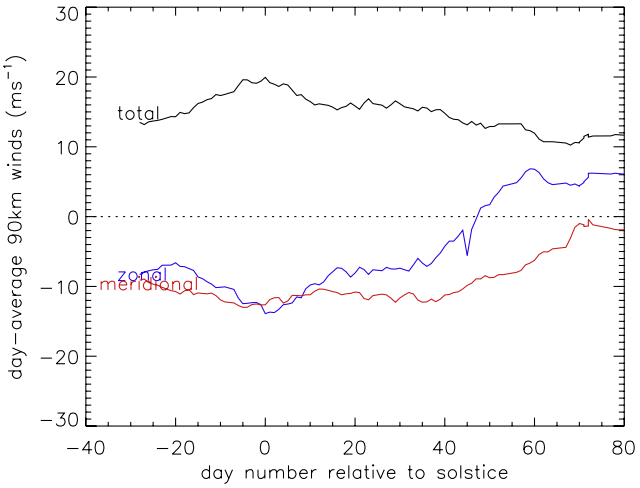

Figure 3. Winds at 90 km altitude for the summer of 2008, as determined by NSMR. For clarity, the underlying time series of daily means have been smoothed with a 10-day wide Lee filter.

[11] The NSMR system also delivers horizontal wind values, typically as daily means [e.g., *Tsutsumi et al.*, 1999] and results akin to those shown here but for around 70°N are given by *Manson et al.* [2004]. Figure 3 shows the zonal and meridional components and total wind speed for the summer period and for 90 km altitude obtained from daily mean values. In Figure 3 the daily means have been smoothed by a 10-day wide Lee filter to better show the seasonal variation. The upper reaches of the mesospheric jet are seen in the zonal component until the transition 48 days after solstice. Surprisingly, we see outflow from the pole during the entire period irrespective of the zonal circulation: during the westward phase there is outflow and therefore the flow is quasi-geostrophic while after the zonal wind turns eastward the flow is ageostrophic; see *Hall et al.* [2003b] for more discussion on this.

3. Interpretation

[12] First, we have compared the PMSE characteristics with the 90 km temperature. Again, we should stress that the

meteor radar derived temperatures are poorly calibrated for summer relative to winter, no LIDAR observations having been available since those made by *Höffner and Lübken* [2007]. It is therefore somewhat inexact to compare the absolute values with PMSE onset and disappearance and with the frost point. Moreover, the frost point temperature shown in Figure 2 is for solstice, although we have indicated it as a constant temperature over the entire period. A number of recent studies have indicated the frost point but earlier work, for example, that of *Reid* [1975], illustrates the complexity of this parameter. Furthermore, G. Witt (personal communication, ~1990) has suggested that a more appropriate temperature for ice formation is 120 K because temperatures lower than the nominal frost point are required to overcome the Kelvin barrier [e.g., *Keesee*, 1989] for formation of macro ions. This 120 K criterion is also shown in Figure 2 as mentioned earlier. Therefore let us turn our attention from the PMSE occurrence in relation to the temperature itself and examine the PMSE characteristics and their response to relative temperature changes. We have constructed scatterplots of the PMSE characteristics as functions of the approximate temperature (Figure 4). For the overall occurrence rate (d^{-1} over height interval 82–92 km) the excursions for rates <0.5% are due to the "tails" in the Lee-filtered time series and can essentially be disregarded, the same being the case for rates <0.2% at 90 km only. While it is no surprise that there is more PMSE when the temperature is lower, here we can identify a clear dependence: a 7 K drop in temperature results in 1% increase in overall (daily) occurrence, and a 12 K drop in temperature is required for 1% increase in occurrence at 90 km only (uncertainty in the temperature change is 10% in each case). In performing linear fits to the data we have excluded occurrence rates <0.5% for the whole height range (Figure 4, top) and <0.2% for 90 km (Figure 4, middle). While these changes seem small compared to the associated temperature changes, note that the overall occurrence rate is of the order of only 2% d^{-1} (see Figure 2) and never exceeds 6% with somewhat lower values for 90 km only. Thus, as an example, a rise in temperature of 7 K could conceivably halve the overall number of echoes in the regime observed by the radar. Although not the focus of this study, it is interesting to note the periodicity evident in the occurrence rates shown in Figure 2. Similar 4- and 10-day (etc.) periodicities are seen in mesospheric dynamics at several scales [*Hall et al.*, 2003a]. We can therefore anticipate varying advection of cold/warm air (likely due to long period waves), heating due to turbulent energy dissipation and appearance/disappearance of turbulent structures, all of which would modulate PMSE occurrence. Periodicities in the occurrence rates such as those seen in Figure 2 have previously been reported and partially explained by *Kirkwood et al.* [2002].

[13] A somewhat less well-known result is that the preferred PMSE altitude varies with temperature, as shown in Figure 4 (bottom), namely, 1 km per 5 K (yet again 10% uncertainty). It is currently accepted that the mesopause at 78°N in summer lies in the vicinity of 90 km [*Lübken and Müllemann*, 2003]. The varying temperature observed by NSMR can therefore be interpreted as a deepening/reduction of the mesopause temperature minimum itself. A consequence would be that an increase of the environmental lapse rate (by "pulling" the mesopause to a lower temperature) would decrease both static and dynamic stability of the upper mesosphere and therefore encourage turbulence. The resulting shifting of the corresponding temperature profile in the underlying mesosphere will also cause the criterion for macroion, including charged-aerosol, formation, and thus PMSE occurrence [*Cho et al.*, 1992], to change height. A future investigation, therefore, might be to see if turbulent intensity at the PMSE preferred height increases toward the origin in Figure 4 (bottom). On the other hand, other observations (e.g., summarized by *Hall et al.* [1999]) indicate that in summer, little turbulence is present in the midmesosphere, but considerable turbulence characterizes the mesopause region where gravity waves propagating from the troposphere break on the "steep beach" of the lower thermosphere [*McIntyre*, 1989].

[14] From Figures 2 and 3 it can be seen that around day 50 after solstice, the zonal wind reverses from westward to eastward, the day-average temperature increases up to 115 K (but recall the uncertainty in absolute values) and PMSE occurrence rate becomes close to zero. If this reversal could be considered indicative of cyclonic flow round the pole, one would expect an associated poleward advection of warmer air. Therefore, in a similar fashion to the comparison with temperature, we have constructed scatterplots of the three PMSE characteristics (occurrence, occurrence at 90 km, and preferred altitude) and meridional wind components for 90 km altitude, shown in Figure 4. Comparisons of characteristics with the zonal wind are shown in Figure 5 (left), and with the meridional wind in Figure 5 (right). Having first removed periodicities $\leq$5 days using a Lee filter, we have again performed linear fits for percentages of day and observed height interval >0.5%, and for percentages of day at 90 km only >0.2%. For the whole height interval (Figure 5, top), a 1% increase in occurrence is associated with a 7.3 ± 0.8 m s^{-1} increase westward and a 1.1 ± 0.3 m s^{-1} increase equatorward. At 90 km only (Figure 5, middle), a 1% increase in occurrence is associated with a 13.7 ± 1.5 m s^{-1} increase westward and a 1.9 ± 0.6 m s^{-1} increase equatorward. As we see in Figure 5 (bottom), there is no obvious correlation between winds and occurrence height and the fits are not shown here since the errors exceed 100%.

[15] Relationships between equatorward flow and PMSE occurrence have been noted earlier by, for example, *Morris et al.* [2006, 2007] and *Latteck et al.* [2008]; here we have attempted to quantify the relationship, at least for 78°N, 16°E. The westward flow, associated with high pressure in the polar cap region, is quasi-geostrophic, Rayleigh drag causing an equatorward component. If the equatorward flow is zonally representative, there will be a resulting divergence from the pole causing an upwelling and therefore adiabatic cooling. This in turn would presumably be responsible for increasing the PMSE occurrence as the mesosphere cools and/or colder air is advected equatorward. While a very plausible hypothesis, and supported by similar more qualitative observations from other locations, simultaneous high-latitude observations at suitably spaced longitudes will be required for proof.

4. Conclusions

[16] First, we have demonstrated the capability of the refurbished SOUSY Svalbard MST Radar (SSR2), and

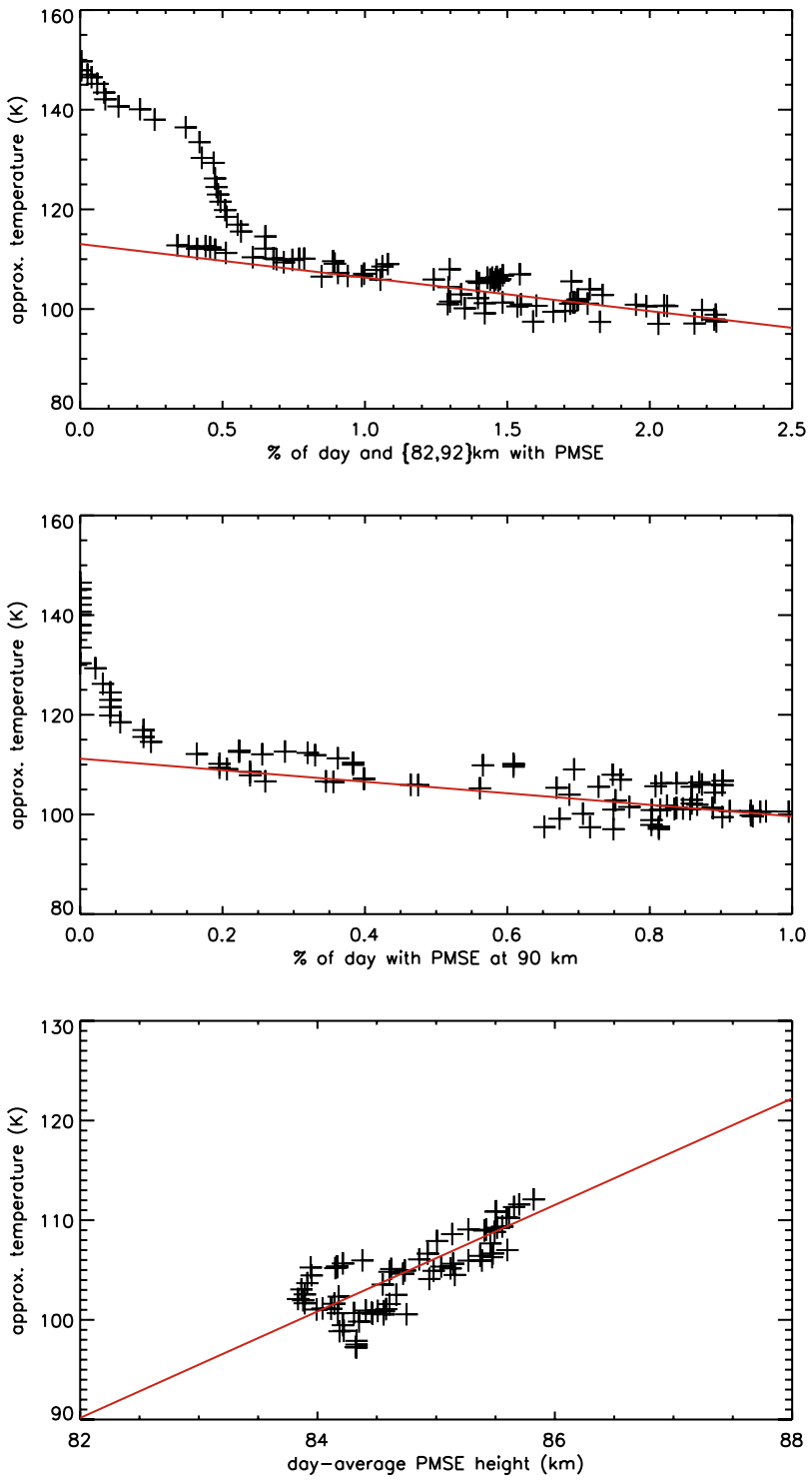

Figure 4. (top) Scatterplot of 90-km temperature versus daily PMSE occurrence in the interval 82–92 km, (middle) scatterplot of 90-km temperature versus daily PMSE occurrence at 90 km only, and (bottom) scatterplot of 90-km temperature versus daily PMSE preferred altitude. In all cases a minimum absolute deviation linear fit has been applied, shown by the solid lines.

how a low-power system can provide useful information on mesospheric features such as PMSE. Although outside the scientific scope of this study, the system can simultaneously monitor the tropopause height, frontal passages, tropopause folding, etc., which may in future studies provide insight into forcing of the upper atmosphere by gravity waves originating lower down. Owing to very modest transmitted power, the system can safely operate unattended and therefore monitor the onset, development and demise of PMSE through the polar summer months.

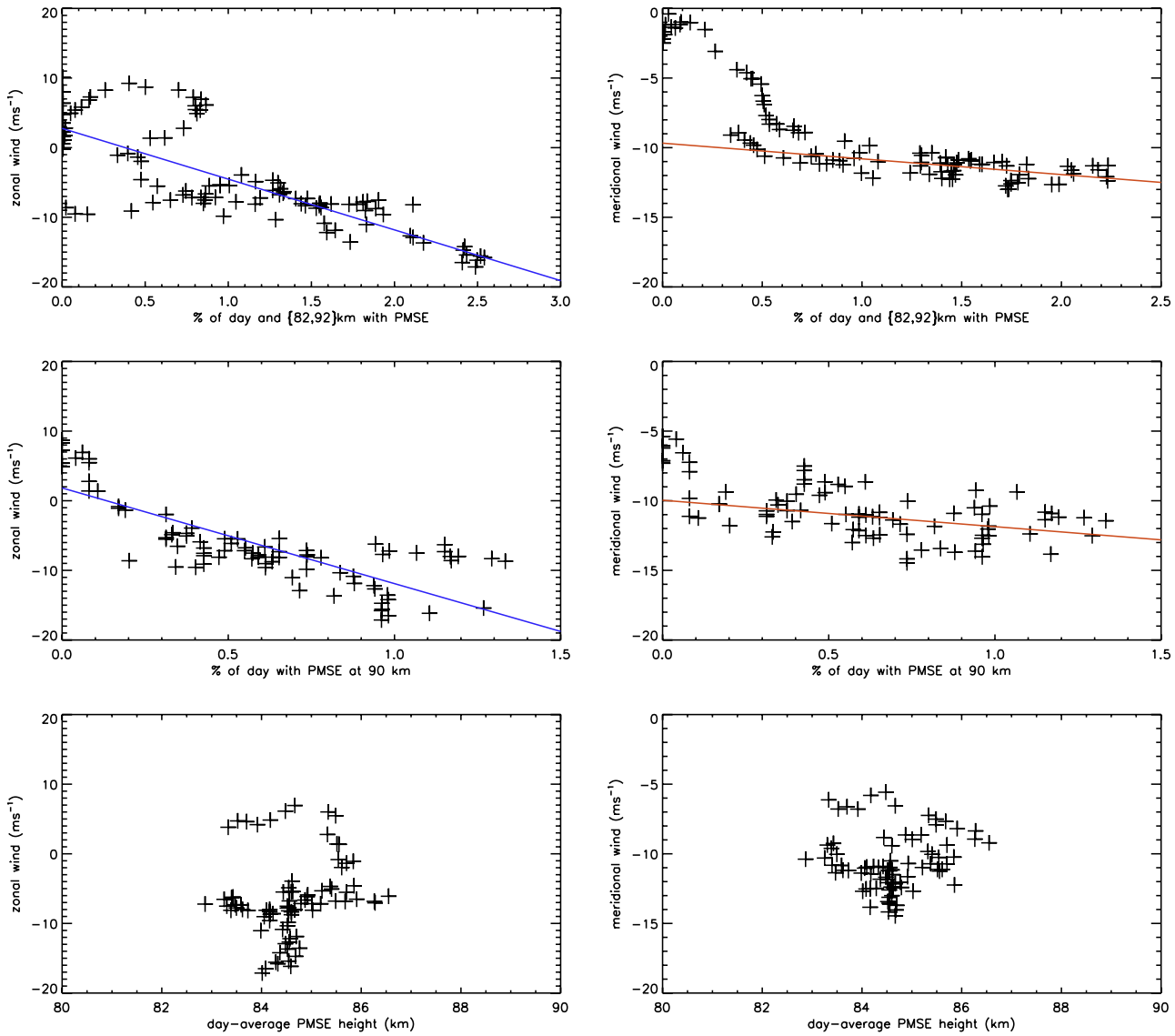

Figure 5. Comparisons of 90-km winds with the three PMSE characteristics. (left) Comparisons with zonal wind and (right) comparisons with meridional wind. (top) Comparison of winds with daily occurrence rates for the interval 82–92 km, (middle) comparisons with occurrence rates at 90 km only, and (bottom) comparison with preferred altitude. For the occurrence rates, linear fits are shown by straight lines, but these are omitted for the preferred height scatterplots since there is little or no correlation here. A 5-day Lee filter smoothing was applied to the wind time series prior to linear fitting.

[17] In this study we have combined the SSR2 observations, here in terms of daily occurrence rates and preferred heights, with 90 km wind and temperature data from a colocated meteor wind radar (NSMR) indirectly supported by nearby optical instruments. Temperature drops cause increases in PMSE occurrence: for the height interval 82–92 km, a decrease of around 7 K increases the occurrence, typically, by 1–2% d^{-1}. A similar increase in occurrence is found for a 1 m s^{-1} increase in equatorward wind (comparison of temperature and wind components being superfluous since these parameters are interdependent). A temperature drop of 5 K at 90 km altitude results in a lowering of the underlying preferred PMSE altitude by 1 km. Using radar backscatter power observations alone, this study has therefore qualified, at least for 78°N, 16°E and 2008, the dependence of PMSE occurrence rates and preferred heights on 90-km neutral temperature and dynamics.

[18] **Acknowledgments.** The authors are indebted to the Norwegian Amundsen Centre for economic support for the SSR2 radar, which is a donation by the Max Planck Institute in Lindau to the University of Tromsø. We also appreciate the support of Charles Deehr and the Optical group at the Geophysical Institute, University of Alaska Fairbanks, which owns the optical instrument used to obtain the OH rotational temperatures. Finally, the authors would like to express gratitude for the help and support of the Jicamarca staff, in particular the members of the Electronics and Instrumentation group and Victor Quesada. Truls Lynne Hansen suggested the interesting analogy between PMSE and a rainbow.

References

Brattli, A., Ø. Lie-Svendsen, K. Svenes, U.-P. Hoppe, I. Strelnikova, M. Rapp, T. Latteck, and M. Friedrich (2009), The ECOMA 2007 campaign: Rocket observations and numerical modelling of aerosol par-

ticle charging and plasma depletion in a PMSE/NLC layer, *Ann. Geophys.*, *27*, 781–796.
Cho, J. Y. N., and J. Röttger (1997), An updated review of polar mesosphere summer echoes: Observations, theory and their relations to noctilucent clouds and subvisible aerosols, *J. Geophys. Res.*, *102*, 2001–2020, doi:10.1029/96JD02030.
Cho, J. Y. N., T. M. Hall, and M. C. Kelley (1992), On the role of charged aerosols in polar mesosphere summer echoes, *J. Geophys. Res.*, *97*, 875–886.
Czechowsky, P., R. Rüster, and G. Schmidt (1979), Variations of mesospheric structures in different seasons, *Geophys. Res. Lett.*, *6*, 459–462, doi:10.1029/GL006i006p00459.
Dyrland, M. E., and F. Sigernes (2007), An update on the hydroxyl airglow temperature record from the Auroral Station in Adventdalen, Svalbard (1980–2005), *Can. J. Phys.*, *85*, 143–151, doi:10.1139/P07-040.
Ecklund, W. L., and B. B. Balsley (1981), Long-term observations of the Arctic mesosphere with the MST radar at Poker Flat, Alaska, *J. Geophys. Res.*, *86*, 7775–7780, doi:10.1029/JA086iA09p07775.
Hall, C. M., and J. Röttger (2001), Initial observations of polar mesospheric summer echoes using the EISCAT Svalbard radar, *Geophys. Res. Lett.*, *28*, 131–134, doi:10.1029/2000GL003821.
Hall, C. M., U. P. Hoppe, T. A. Blix, E. V. Thrane, A. H. Manson, and C. E. Meek (1999), Seasonal variation of turbulent energy dissipation rates in the polar mesosphere: A comparison of methods, *Earth Planet. Space*, *51*, 515–524.
Hall, C. M., T. Aso, and M. Tsutsumi (2002), An examination of high latitude upper mesosphere dynamic stability using the Nippon/Norway Svalbard Meteor Radar, *Geophys. Res. Lett.*, *29*(8), 1280, doi:10.1029/2001GL014229.
Hall, C. M., S. Nozawa, C. E. Meek, A. H. Manson, and Y. Luo (2003a), Periodicities in energy dissipation rates in the auroral MLT, *Ann. Geophys.*, *21*, 787–796.
Hall, C. M., T. Aso, A. H. Manson, C. E. Meek, S. Nozawa, and M. Tsutsumi (2003b), High-latitude mesospheric mean winds: A comparison between Tromsø (69°N) and Svalbard (78°N), *J. Geophys. Res.*, *108*(D19), 4598, doi:10.1029/2003JD003509.
Hall, C. M., T. Aso, M. Tsutsumi, J. Höffner, F. Sigernes, and D. A. Holdsworth (2006), Neutral air temperatures at 90 km and 70° and 78°N, *J. Geophys. Res.*, *111*, D14105, doi:10.1029/2005JD006794.
Hocking, W. K. (1999), Temperatures using radar-meteor decay times, *Geophys. Res. Lett.*, *26*, 3297–3300, doi:10.1029/1999GL003618.
Höffner, J., and F.-J. Lübken (2007), Potassium lidar temperatures and densities in the mesopause region at Spitsbergen (78°N), *J. Geophys. Res.*, *112*, D20114, doi:10.1029/2007JD008612.
Holdsworth, D. A., R. J. Morris, D. J. Murphy, I. M. Reid, G. B. Burns, and W. J. R. French (2006), Antarctic mesospheric temperature estimation using the Davis mesosphere-stratosphere-troposphere radar, *J. Geophys. Res.*, *111*, D05108, doi:10.1029/2005JD006589.
Keesee, R. G. (1989), Nucleation and particle formation in the upper atmosphere, *J. Geophys. Res.*, *94*, 14,683–14,692, doi:10.1029/JD094iD12p14683.
Kelley, M. C., D. T. Farley, and J. Röttger (1987), The effect of cluster ions on anomalous VHF backscatter from the summer polar mesosphere, *Geophys. Res. Lett.*, *14*, 1031–1034, doi:10.1029/GL014i010p01031.
Kirkwood, S., V. Barabash, B. U. E. Brändström, A. Moström, K. Stebel, N. Mitchell, and W. Hocking (2002), Noctilucent clouds, PMSE and 5-day planetary waves: A case study, *Geophys. Res. Lett.*, *29*(10), 1411, doi:10.1029/2001GL014022.
Latteck, R., W. Singer, R. J. Morris, W. K. Hocking, D. J. Murphy, D. A. Holdsworth, and N. Swarnalingam (2008), Similarities and differences in polar mesospheric summer echoes observed in the Arctic and Antarctica, *Ann. Geophys.*, *26*, 2795–2806.
Lee, J. S. (1986), Speckle suppression and analysis for synthetic aperture radar images, *Opt. Eng.*, *25*, 636–643.
Lübken, F.-J., and A. Müllemann (2003), First in situ measurements in the summer mesosphere at very high latitudes (78°N), *J. Geophys. Res.*, *108*(D8), 8448, doi:10.1029/2002JD002414.
Lübken, F.-J., M. Zecha, and J. Höffner (2004), Temperatures, polar mesosphere summer echoes, and noctilucent clouds over Spitsbergen (78°N), *J. Geophys. Res.*, *109*, D11203, doi:10.1029/2003JD004247.
Manson, A. H., C. E. Meek, C. M. Hall, S. Nozawa, N. J. Mitchell, D. Pancheva, W. Singer, and P. Hoffmann (2004), Mesopause dynamics from the Scandinavian triangle of radars within the PSMOS-DATAR project, *Ann. Geophys.*, *22*, 367–386.
McIntyre, M. E. (1989), On dynamics and transport near the polar mesopause in summer, *J. Geophys. Res.*, *94*, 14,617–14,628, doi:10.1029/JD094iD12p14617.
Morris, R. J., D. J. Murphy, R. A. Vincent, D. A. Holdsworth, A. R. Klekociuk, and I. M. Reid (2006), Characteristics of the wind, temperature and PMSE field above Davis, Antarctica, *J. Atmos. Sol. Terr. Phys.*, *68*, 418–435, doi:10.1016/j.jastp.2005.04.011.
Morris, R. J., D. J. Murphy, A. R. Klekociuk, and D. A. Holdsworth (2007), First complete season of PMSE observations above Davis, Antarctica, and their relation to winds and temperatures, *Geophys. Res. Lett.*, *34*, L05805, doi:10.1029/2006GL028641.
Rapp, M., and F.-J. Lübken (2004), Polar mesospheric summer echoes (PMSE): Review of observations and current understanding, *Atmos. Chem. Phys.*, *4*, 2601–2633.
Reid, G. (1975), Ice clouds in the summer polar mesopause, *J. Atmos. Sci.*, *32*, 523–535, doi:10.1175/1520-0469(1975)032<0523:ICATSP>2.0.CO;2.
Robinson, T. R., T. K. Yeoman, R. S. Dhillon, M. Lester, E. C. Thomas, J. D. Thornhill, D. M. Wright, A. P. van Eyken, and I. W. McCrea (2006), First observations of SPEAR-induced artificial backscatter from CUTLASS and the EISCAT Svalbard radars, *Ann. Geophys.*, *24*, 291–309.
Röttger, J. (2001), Observations of the polar D-region and the mesosphere with the EISCAT Svalbard radar and the SOUSY Svalbard radar, in *Environmental Research in the Arctic*, *Mem. Natl. Inst. Polar Res.*, *4*, 9–20.
Röttger, J., M. Rapp, J. Trautner, A. Serafimovich, and C. M. Hall (2007), New PMSE observations with the EISCAT 500 MHz Svalbard radar and the SOUSY 53.5 MHz radar, in *Proceedings of the 11th MST-Radar Workshop*, *McMillan Adv. Res. Ser.*, pp. 136–140, Macmillan, New York.
Tsutsumi, M., D. Holdsworth, T. Nakamura, and I. Reid (1999), Meteor observations with an MF radar, *Earth Planets Space*, *51*, 691–699.
von Zahn, U., and J. Berger (2003), Persistent ice cloud in the midsummer upper mesosphere at high latitudes: Three-dimensional modeling and cloud interactions with ambient water vapor, *J. Geophys. Res.*, *108*(D8), 8451, doi:10.1029/2002JD002409.
Wannberg, G., et al. (1997), The EISCAT Svalbard radar: A case study in modern incoherent scatter radar design, *Radio Sci.*, *32*(6), 2283–2307, doi:10.1029/97RS01803.
Woodman, R. F., G. Michhue, J. Röttger, and O. Castillo (2007), The MPI-SOUSY-VHF radar at Jicamarca: High altitude resolution capabilities, in *Proceedings of the 11th MST-Radar Workshop*, *McMillan Adv. Res. Ser.*, pp. 317–334, Macmillan, New York.

J. L. Chau and K. Kuyeng, Radio Observatorio de Jicamarca, Instituto Geofisico del Peru, Apartado 13-0207, Lima 13, Peru. (jchau@jro.igp.gob.pe; kkuyeng@jro.igp.gob.pe)
M. Dyrland, University Centre in Svalbard, N-9171 Longyearbyen, Norway. (margit.dyrland@unis.no)
C. M. Hall, Tromsø Geophysical Observatory, University of Tromsø, N-9037 Tromsø, Norway. (chris.hall@uit.no)
J. Röttger, Max Planck Institute for Solar System Research, Max-Planck-Strasse 2, D-37191 Katlenburg-Lindau, Germany. (roettger@mpg.de)
M. Tsutsumi, National Institute of Polar Research, 1-9-10 Kaga, Itabashi, Tokyo 173-8515, Japan. (tutumi@nipr.ac.jp)